The Effect of Partial Baffles on Natural Convection in an Inclined Rectangular Enclosure PART II: Numerical Solution

by PAUL K.-B. CHAO*, HIROYUKI OZOE**, NOAM LIOR*** and STUART W. CHURCHILL***

Abstract

Theoretical results were obtained by finite-difference solutions for 2 x 1 x 1 enclosures with one partial baffle extending between the 2 x 1 heated and cooled surfaces. The computations were for $Ra = 6000$, $Pr = \infty$, several baffle locations, breadths, thicknesses and conductivities, and a complete range of inclinations about the shorter dimension of the enclosure. The mean Nusselt number and representative streaklines are presented for each condition. The results are in good qualitive agreement with the experimental results of Part 1 for slightly different conditions. The calculations reveal that increasing the conductivity of the baffle reduces the heat flux through the fluid significantly for inclinations less than the critical value for transition in the mode of circulation.

Long Synopsis

Theoretical results are presented for the effect of a partial baffle on natural convention inside an inclined rectangular enclosure. The results are limited to a 2 x 1 x 1 enclosure heated isothermally on the lower 2 x 1 surface and cooled isothermally on the opposing surface. The four side-walls were postulated to be perfect insulators. The baffle was parallel to the 1 x 1 surfaces and extended from the heated to the cooled surface.

A finite-difference method was used to solve the equations for the conservation of mass, momentum and energy in three dimensions.

Most prior theoretical investigations of natural convection in enclosures have postulated two-dimensional motion. However, three-dimensionality is significant in all finite enclosures and is the controlling factor in the transitions in the mode of circulation and hence in the rate of heat transfer.

The solutions were limited to a Rayleigh number of 6000 and an asymptotically large Prandtl number. However, prior experimental and theoretical results indicate that the pattern of circulation, the Nusselt number, and their variation with the angle of inclination do not depend significantly on the Prandtl number for values greater than 0.7 in this range of the Rayleigh number. Furthermore, the pattern of circulation and the relative dependence of the Nusselt number on the angle of inclination are known to be relatively independent of the Rayleigh number over a moderate range about the chosen value. Hence the results herein are presumed to be representative for all large Prandtl numbers and a moderate range of the Rayleigh number.

This theoretical work was carried out in direct support of the experimental work reported in a companion paper [1]. The primary objective of both studies was to investigate the possible use of partial baffles to suppress convective heat transfer in solar collectors.

The mathematical model and method of solution previously developed and utilized by the present investigators was adapted to account for the presence of the baffles. This model postulates the Boussinesq simplifications and utilizes the vector potential and vorticity. A steady-state solution was obtained by transient calculations using the ADI (alternating-direction-implicit) method with a false-transient term for the vector potential. A 10 x 10 x 20 grid was used for the fluid with additional grid points for the baffles. The computed velocity field was used to compute streaklines. The corresponding particle paths were displayed dynamically on a cathode ray tube. Photographs of some of these displays are included in the full paper. The average Nusselt number for convection, and the incremental value due to conduction to the cooled wall from the baffle were also computed.

Calculations were carried out for two baffle breadths, two baffle thicknesses, 3 baffle locations, a complete range of ratios of the conductivity of the baffle to that of the fluid, and a complete gamut of inclinations about the shorter dimension of the enclosures as an axis.

The theoretical and experimental results are in good agreement with respect to the patterns of circulation and the transition from one mode to another despite large differences in the Rayleigh and Prandtl numbers. However, these differences preclude quantitative comparison of the rates of heat transfer. The theoretical calculations provide much more detail, clarity and precision than the experimental results, particularly with respect to the patterns of flow. This additional information is thereby very useful in interpreting the thermal behavior. Investigating such effects as baffle thickness and conductivity is much easier theoretically than experimentally.

The baffles were found to have relatively little effect for the horizontal orientation of the heated surface. However, they drastically modified the orientation and even the number of roll-cells for inclinations of the horizontal surface. The path of circulation was generally extended by a baffle. The increased drag owing to this longer path, as well as the drag of the baffle itself, reduced the rate of circulation and hence the rate of heat transfer.

The principal results are for a baffle extending half way across the enclosure. The results for a 7/10-th extension were similar. Locations at 1/4, 1/2 and 3/4 of the distance between the 1 x 1

* Mobil Research and Development Corporation, Paulsboro, NJ 08066, USA
** Department of Industrial and Mechanical Engineering, Okayama University, Okayama, Japan
*** The University of Pennsylvania, Philadelphia, PA 19104, USA

ends were investigated. The flow patterns differed significantly. The difference between the 1/4 and 3/4 locations suggests the possibility of multiple stationary states depending on the conditions, and hence the initial direction of circulation. The thickness and conductivity of the baffle had only slight effects on the circulation.

As indicated in Figure 1 (26), the Nusselt number was reduced significantly for all inclinations by a half-extended baffle, but, as indicated in Figure 2 (28), only slightly more by the 7/10-th extended baffle. As indicated in Figure 3 (29), locations of the baffle near the elevated end produced the greatest reduction, followed by location near the unelevated end, but the central location produced the greatest reduction for large inclinations. Figure 4 (27) reveals that increasing the conductivity of the baffle shifts the minimum in the Nusselt number to smaller inclinations, reducing its value for small inclinations, but increasing it for high ones. As seen in Figure 4, increasing the thickness of the baffle has the same effect as increasing its conductivity. This indicates that conduction across the baffle from one roll-cell to another has a greater effect on the flow pattern, and hence on heat transfer through the fluid, than conduction along the baffle.

It is concluded that the theoretical method of solution described herein produces reliable and detailed predictions of natural convection in inclined, baffled enclosures. Such results provide greater insight into the behavior than experimental measurements alone.

The overall conclusion of the combined and theoretical investigation is that partial baffles can be used to modified the pattern of circulation and thereby significantly reduce the heat flux through the fluid.

Reference

Chao, Paul and K.-B., Ozoe, H., Lior, H., and Churchill, S.W., The Effect of Partial Baffles on Natural Convection in an Inclined Rectangular Enclosure. Part I. Experimental Observations. *Chem. Eng. Fundam.* in this paper.

Introduction

The work reported herein is part of a continuing investigation of natural convection in enclosures, one application of which is the reduction of heat losses across the air film in solar collectors. The specific objective of the current work is to investigate the effect of partial baffles in suppressing heat transfer. The experimental phase of the investigation was described in a companion paper [1]. The supporting theoretical work is presented herein. Prior related work, both experimental and theoretical, was discussed in the former paper. It is therefore sufficient to note that prior theoretical work for partial baffles is limited to two-dimensional convection in enclosures, heated and cooled on the vertical sides. Our research in concerned with finite enclosures heated from below and inclined. Three-dimensionality is not only significant in all real, finite enclosures; it is generally the controlling factor.

Controlled variation of the many parameters of the problem – the Rayleigh number, the Prandtl number, the two aspect rations and two inclinations of the enclosure, and the breadth, thickness and location of the baffles – is more convenient and economical with the theoretical model than with the experimental apparatus. The calculations produce far more detailed information than the experiments. Furthermore, non-isothermality in the heated and cooled surfaces, and heat conduction along and through the "adiabatic surfaces" affect the motion significantly in all experiments. Hence, the objective of the combined work is to confirm the validity of the theoretical calculations for representative conditions and thereby establish reasonable confidence in the results for others.

Conditions

The theoretical calculations were for a 2 x 1 x 1 rectangular enclosure with uniform dimensionless temparatures of 0.5 and −0.5 on the lower and upper 2 x 1 surfaces, respectively, and perfectly insulated side walls. Solutions were obtained for two baffle breadths, two baffle thickness, three baffle locations, a complete series of baffle/fluid conductivity ratios, ranging from perfect insulators to perfect conductors, and a series of inclinations of the longer dimension (that is, about the shorter dimension as an axis) from 0 to 2π rad. All of the calculations were for $Pr \to \infty$ and $Ra = 6000$. The baffle breadths and locations correspond to a selection of the experimental conditions described in Part I.

Finite Difference Method

The mathematical model and process of solution, other than for the baffles and for the boundary condition on the x-component of the vector potential, were equivalent to that used by Ozoe, et al. [2] and hence will not be reproduced in detail. In summary, the idealizations of Boussinesq were postulated, the equations were dedimensionalized and then transformed by introduction of the vector potential and the vorticity. Following Samuels and Churchill [3], a false transient term was introduced in the equation relating the vector potential to the vorticity to transform this expression from elliptic form to the parabolic form of the vorticity and energy equations.

The coordinates for the model and for the finite-difference calculations are indicated in Figure 1. X is the dimensionless distance in the long dimension of the enclosure as measured from one end, Y is measured from the side wall containing the baffle, and Z is measured from the cooled surface. The axis of inclination was $X = 0$, $Z = 1$.

In prior analyses, the boundary condition of zero velocity on all of the surfaces was satisfied by setting the normal derivative and the tangential components of the vector potential to zero. In this work such conditions lead to instability in the numerical calculations except for prohibitively small time steps, presumably due to the discontinuity at the free edge of the baffle. Setting the X-component of the vector potential equal to zero on the baffle, and for convenience, on the $X = 0$ and $X = 2$ surfaces as well, resulted in a more rapid convergence of the calculations to the steady state.

A uniform grid size of 0.1 was used for all of the calculations resulting in 21 x 11 x 11 = 2541 grid points, numbered as indicated. The plane of the baffle was designated as I = NXF with its tip at J = NYF. For all of the calculations the baffle extended to and was in contact with the heated and cooled surfaces ($Z = 0,1$).

The temperature is not equal on the opposing sides of a perfectly insulated baffle for unsymmetrical conditions. Hence, separate values were assigned as indicated. A third value is necessary at the tip.

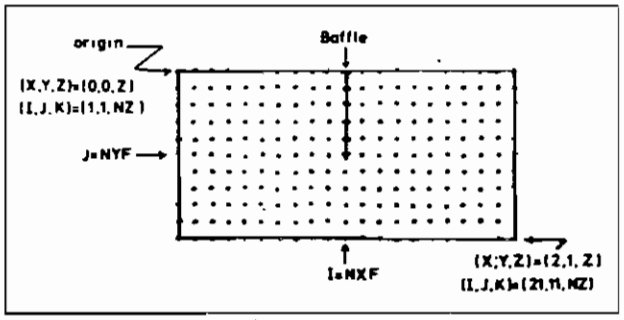

Fig. 1 Grid spacing and notation

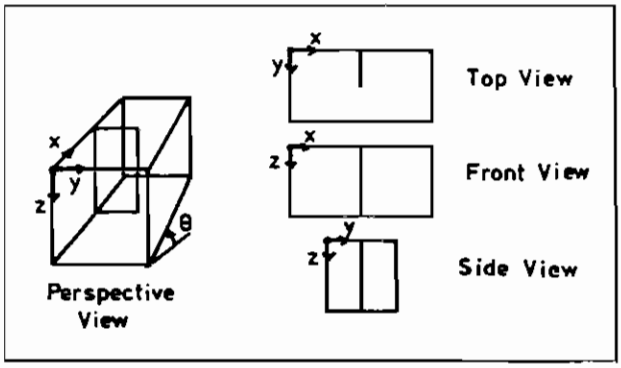

Fig. 2 Viewing angle and coordinates for streakline displays

The temperature of a perfectly conducting baffle varies linearly between the heated and cooled surfaces. In terms of the grid points,

$$T_{NXF,J,K} = \frac{K}{10} - 0.6 \qquad \begin{matrix} J = 1,2, \ldots NYF \\ K = 1,2, \ldots 11 \end{matrix} \tag{1}$$

The temperatures on a baffle of finite conductivity were updated one step behind the energy, vorticity and velocity calculations using the following scheme.

The temperature variation across the thickness of the baffle was postulated to be negligible. The energy balance over a finite element of the baffle can then be expressed as

$$\frac{H^2}{\alpha_w}\frac{\delta T}{\delta t} = \delta_Z^2 T + \delta_Y^2 T + \frac{\lambda_f H}{\lambda_w L}\Delta X\, \delta_X^2 T \tag{2}$$

where here

$$\delta_X^2 T = (T_{i+1,j,k} - 2T_{i,j,k} + T_{i-1,j,k})/(\Delta X)^2 \tag{3}$$

$$\delta_Z^2 T = (T_{i,j,k+1} - 2T_{i,j,k+1} + T_{i,j,k-1})/(\Delta Z)^2 \tag{4}$$

The corresponding expression for the y-direction depends on J. For J = 1

$$\delta_Y^2 T = 2\,(T_{i,2,k} - T_{i,1,k})/(\Delta Y)^2 \tag{5}$$

while for 1 < J < NYF

$$\delta_Y^2 T = (T_{i,j+1,k} - 2T_{i,j,k} + T_{i,j-1,k})/(\Delta Y)^2 \tag{6}$$

and for J = NYF

$$\delta_Y^2 T = 2\left[T_{i,j-1,k} - \left(1 + \frac{\lambda_f}{\lambda_w}\right) T_{i,j,k} + \frac{\lambda_f}{\lambda_w} T_{i,j+1,k}\right]/(\Delta Y)^2 \tag{7}$$

In the above

i = NXF
k = 2.3, ... 10
j = NYF

For the horizontal orientation of the enclosure, the stable mode of circulation is known from prior work to consist of two roll-cells with their axes parallel to the shorter horizontal dimension of the enclosure. For the mathematical model, circulation of these roll-cells in either direction is equally probable. In the experimental work, the circulation was always upward near the baffle and downward near the ends owing to a slight nonisothermality in the heated surface. Hence, a thermal shock was imposed as an initial condition for the calculations to induce this direction of circulation.

Streaklines

Representative streaklines were computed from the solution for the velocity field and displayed dynamically on the cathode ray tube of a Vector General 3404 Display Unit using the procedure described by Yamamoto et. al. [4]. Photographs of these displays were taken for four different viewing angles: perspective, top, front and side, as sketched in Figure 2.

Figure 3 shows streaklines for the horizontal orientation with a centrally located, nonconducting baffle of half breadth. A perspective view of representative streaklines at the rear of the enclosure is shown in (a) and at the front in (b). The corresponding end, top and front (rear roll-cells only) views are shown in (c) and (d), (e) and (f), and (g). Streaklines representing the two roll-cells on the left-hand side of (a) and (b) are shown in (h). It is apparent that the circulation consists of four roll-cells with their axes parallel to the shorter horizontal dimension of the enclosure. The two baffle roll-cells on the left-hand side are symmetrical with respect to the plane through the fin to those on the right-hand side. Although not apparent from these photographs, the circulation is up near the central plane and down near the end walls. This pattern differs only slightly from that for no baffle. Frontal and rear streaklines are shown separately in (a)–(g) and left-side ones separately in (h), in part to avoid confusion but also because of the limited capacity of the display unit.

Effect of inclinations

Figure 4 is for a $5\pi/180$ rad inclination with the same baffle. The frontal roll-cell at the unelevated (left-hand) end has enlarged and the rear roll-cell has strengthened since the buoyant force up the heated inclined plate is in coordination with their counterclockwise circulation (as viewed from the front). The axis of the rear roll-cell at the elevated (right-hand) end has rotated almost $45\pi/180$ rad and the frontal right-hand roll-cell has apparently decayed completely owing to the opposition of the buoyant force to their clockwise circu-

lation (as viewed from the front). The development of the circulation with time for an inclination of $5\pi/180$, starting from the steady motion of Figure 3 for no inclination, is illustrated in Figure 5, in which the streaklines are plotted for 356 iterations with a dimensionless time step of 0.001, and for 476 and 703 iterations with a step of 0.01. Figure 4 corresponds to a few more time steps. The left-hand rear roll-cell is seen to spread out axially and then to rotate its axis due to the sudden inclination.

The streaklines for an evaluation of $10\pi/180$ are shown in Figure 6. A single roll-cell now exists across the front of the enclosure with small roll-cells at the rear. The axis of the roll-cell at the rear of the elevated end has rotated π rad, and all three roll-cells are now circulating counterclockwise as viewed from the front, in coordination with the buoyant force.

For an elevation of $20\pi/180$ rad, as shown in Figure 7, the circulation has strengthened but the mode is unchanged. With further strengthening at $60\pi/180$ rad, as shown in Figure 8, the frontal roll-cell no longer penetrates beyond the baffle. Figure 9 shows that for $90\pi/180$ rad of inclination, resulting in heating and cooling on the sides, the baffle apparently causes a slight inclination of the roll-cells with respect to the insulated vertical walls.

Effect of conductivity of baffle

Figures 10–12 are for the conditions of Figures 3, 6 and 8, except that the baffle is perfectly conducting. The effect of conduction in the baffle is to rotate the axes of the rear roll-cells significantly and of the frontal roll-cells slightly for the horizontal orientation, as shown in Figure 10. With inclination, as shown in Figures 11 and 12, the streaklines are similar to those for nonconducting baffles.

The computed streaklines for baffles of a finite thickness ratio $H/L = 100$, and finite conductivity ratios k_s/k_f of 10 and 100 are illustrated in Figure 13 for no inclination. The circulation for the lesser conductivity ratio is seen to be similar to that of Figure 3 for a nonconducting baffle and the circulation for the greater ratio to be similar to that of Figure 10 for a perfectly conducting baffle.

Effect of breadth of baffle

Figures 14–17 show the effect of extending the breadth of the baffle to 7/10th that of the enclosure. This extension does not have a significant effect for no inclination, as shown in Figure 14. However, for an inclination of $5\pi/180$ rad, as illustrated in Figure 15, the frontal roll-cell at the elevated end has vanished; the rear one has changed its direction of circulation by rotating its axis and has linked itself with the left frontal roll-cell. At inclinations of $10\pi/180$ and $60\pi/180$ rad, as shown in Figures 16 and 17, the streaklines have become qualitatively similar to those of Figures 6 and 8 for a half-extended baffle.

Effect of location of baffle

Finally, the effect of location of the baffle is examined in Figures 18–25. The three-quarter location of the baffle at the elevated end produces an oblique and asymmetrical circulation with coalesence of the rear roll-cells even for the horizontal orientation of Figure 18. For $5\pi/180$ rad of inclination, as illustrated in Figure 19, two strong roll-cells are observed on the left in coordination with the buoyant force, and one weak one on the right. For $10\pi/180$ rad, as shown in Figure 10, the axis of this weak roll-cell has become perpendicular to the end of the enclosure, while at $60\pi/180$ rad of inclination, as shown in Figure 21, the frontal left roll-cell has spread across the entire enclosure and the weak roll-cell has become almost parallel.

The results for the one-quarter location of the baffle at the unelevated end are seen in Figures 22–25 to be different from those for the three-quarter location. However, the same pattern was obtainable for no inclination by the reversal of the initial condition, suggesting that multiple stationary states may be possible.

Comparison of theoretical and experimental results

The streaklines of Figures 3–25 are not comparable quantitatively to the photographs of tracer particles in Part I because of slightly different conditions in each case. However, the results are in complete qualitative agreement, i.e., the same modes of circulation are observed. In view of the complex and widely varying patterns of circulation, this agreement is considered to be a strong confirmation of the reliability of the numerical solution.

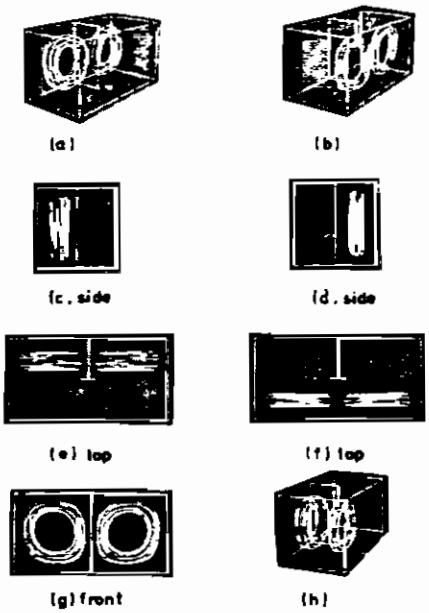

Fig. 3 Streaklines for horizontal orientation with centrally located, half-extended, non-conducting baffle

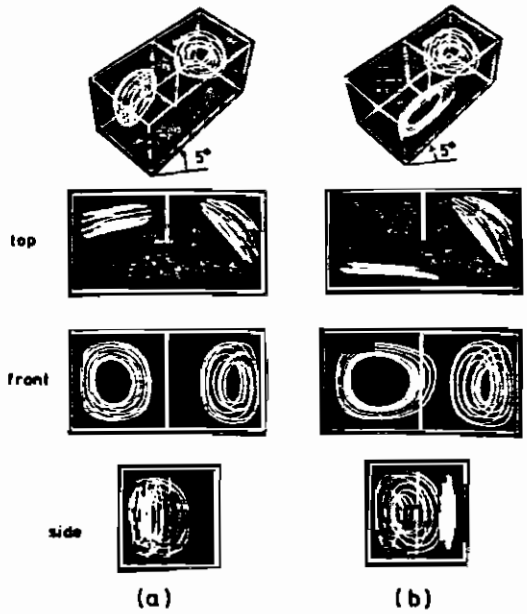

Fig. 4 Streaklines for $5\pi/180$ rad inclination with centrally located, half-extended, non-conducting baffle
a) rear roll-cells
b) left-front and right-rear roll cells

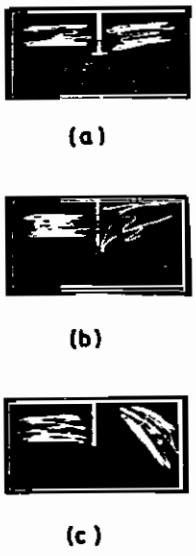

Fig. 5 Transient behavior of streaklines following $5\pi/180$ rad inclination with centrally located half-extended, non-conducting baffle
a) After 356 iterations with $\kappa_t \Delta t/H^2 = 0.001$
b) After 476 iterations with $\kappa_t \Delta t/H^2 = 0.01$
c) After 703 iterations with $\kappa_t \Delta t/H^2 = 0.01$

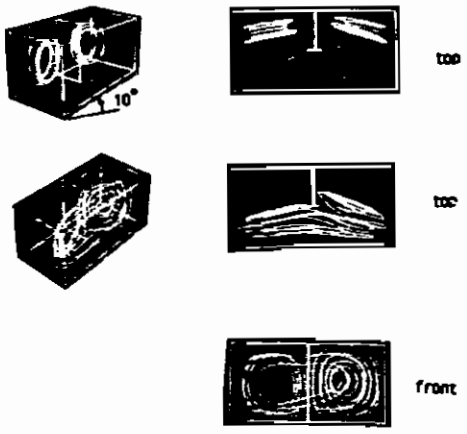

Fig. 6 Streaklines for $10\pi/180$ rad inclination with centrally located, half-extended, non-conducting baffle

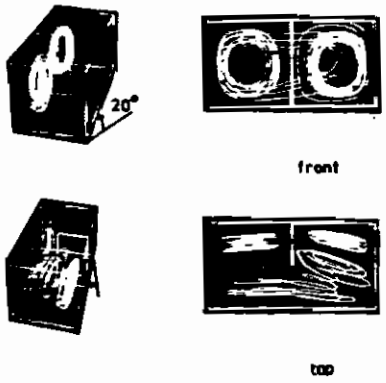

Fig. 7 Streaklines for 20π/180 rad inclination with centrally located, half-extended, non-conducting baffle

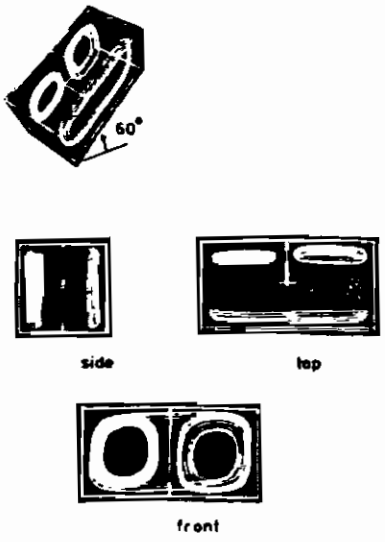

Fig. 8 Streaklines for 60π/180 rad inclination with centrally located, half-extended, non-conducting baffle

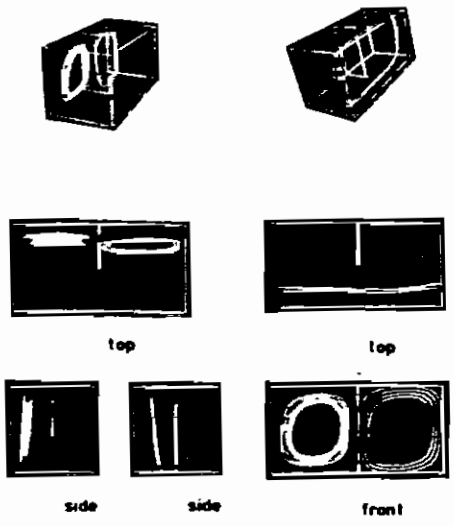

Fig. 9 Streaklines for 90π/180 rad inclinations with centrally located, half-extended, non-conducting baffle

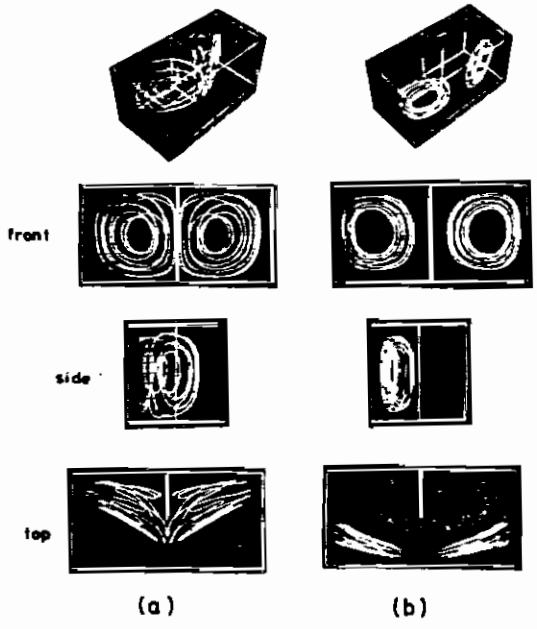

Fig. 10 Streaklines for horizontal orientation with centrally located, half-extended, perfectly-conducting baffle
a) rear roll-cells; b) front roll-cells

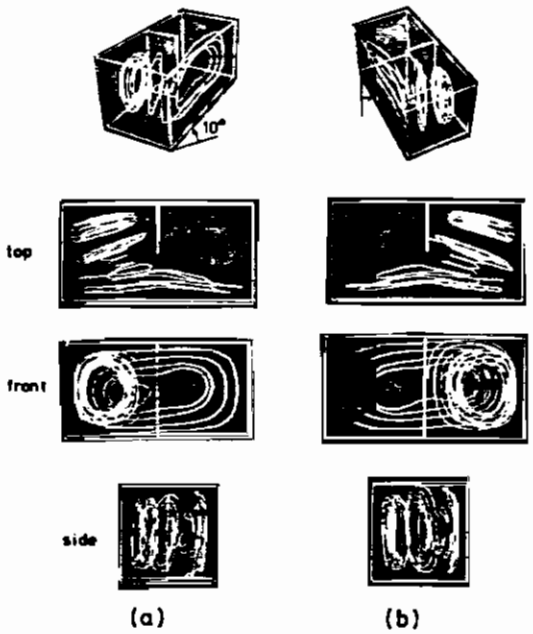

Fig. 11 Streaklines for $10\pi/180$ rad inclination with centrally located, half-extended, perfectly-conducting baffle
a) left roll-cells; b) right roll-cells

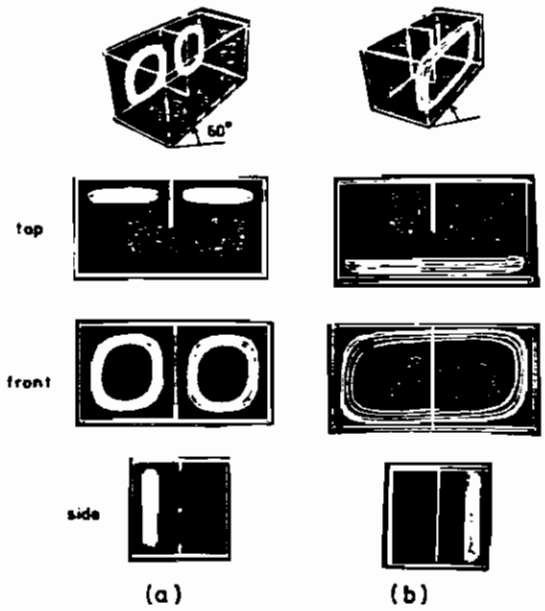

Fig. 12 Streaklines for $60\pi/180$ rad inclination with centrally located, half-extended, perfectly-conducting baffle
a) rear roll cells; b) front roll-cells

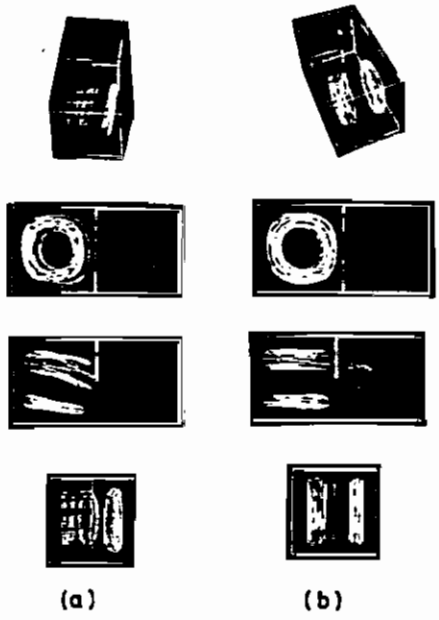

Fig. 13 Streaklines for horizontal orientation with centrally located, half-extended baffle with $H/L = 100$
a) $k_s/k_f = 100$; b) $k_s/k_f = 10$

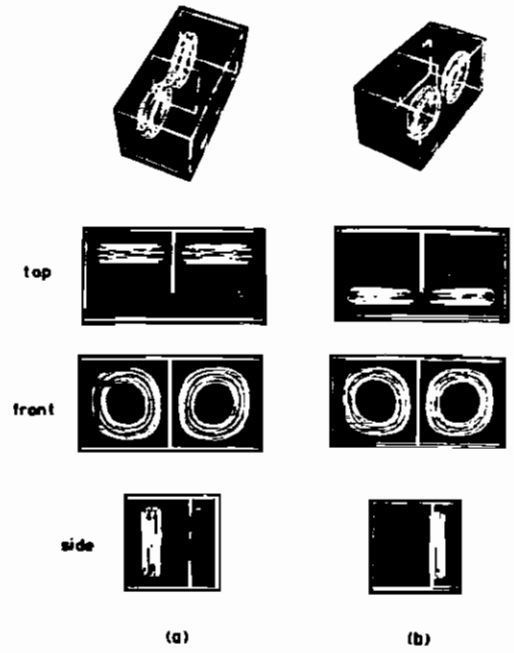

Fig. 14 Streaklines for horizontal orientation with centrally located, 7/10-th extended, non-conducting baffle
a) rear roll-cells; b) front roll-cells

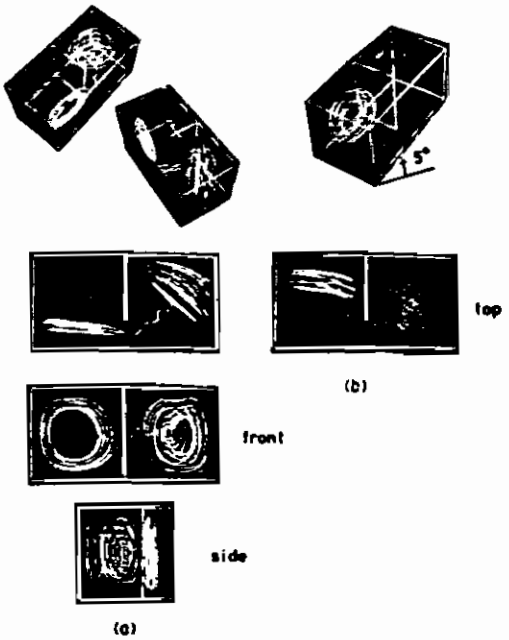

Fig. 15 Streaklines for 5π/180 rad inclination with centrally located, 7/10-th extended, non-conducting baffle
a) left-front and right roll-cells
b) left-rear roll-cells

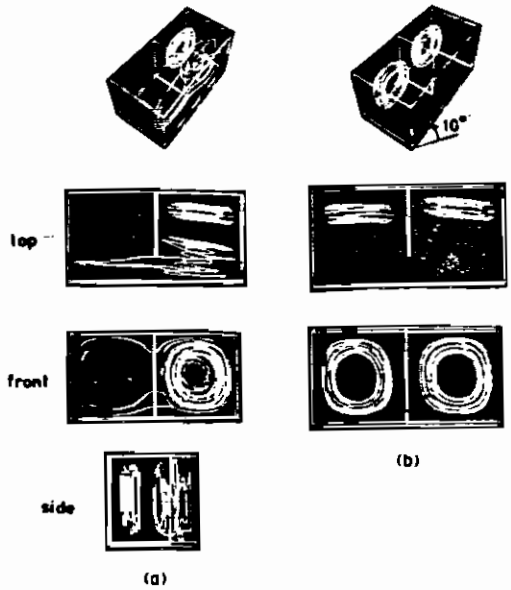

Fig. 16 Streaklines for 10π/180 rad inclination with centrally located, 7/10-th extended, non-conducting baffle
a) right roll-cells; b) rear roll-cells

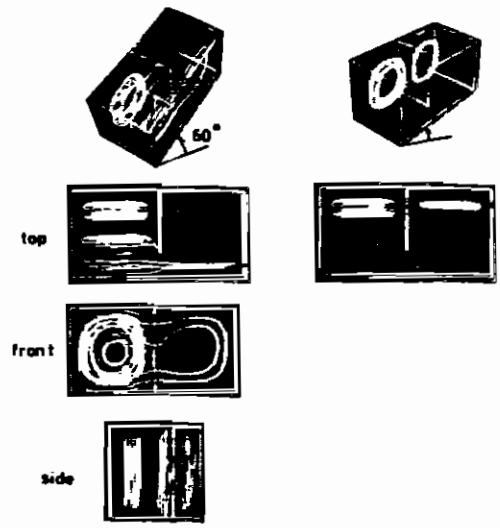

Fig. 17 Streaklines for 60π/180 rad inclination with centrally located, 7/10-th extended, non-conducting baffle
a) left roll-cells; b) rear roll-cells

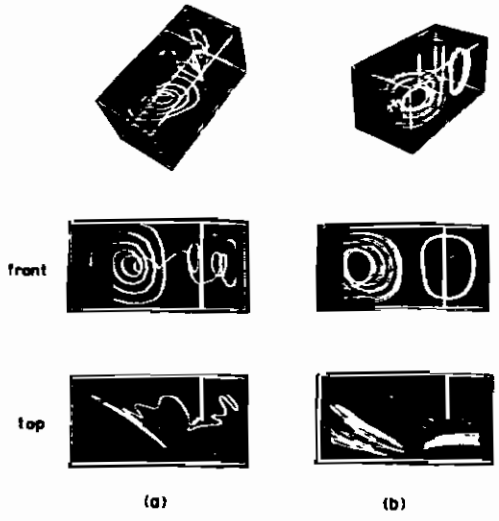

Fig. 18 Streaklines for horizontal orientation with centrally location of half-extended, non-conducting baffle
a) left roll-cells; b) front roll-cells

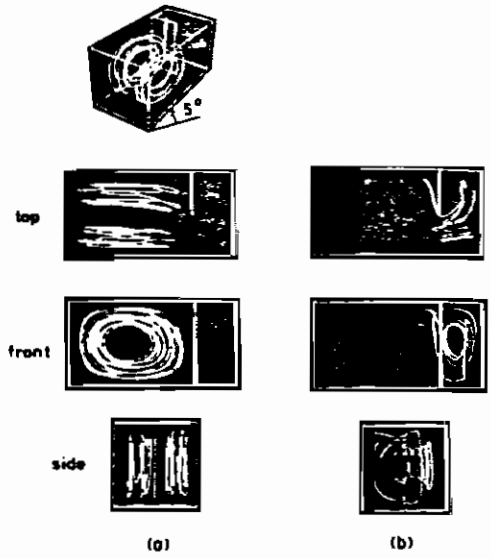

Fig. 19 Streaklines for 50π/180 rad inclination with three-quarter location of half-extended, non-conducting baffle
a) left roll-cells; b) right roll-cells

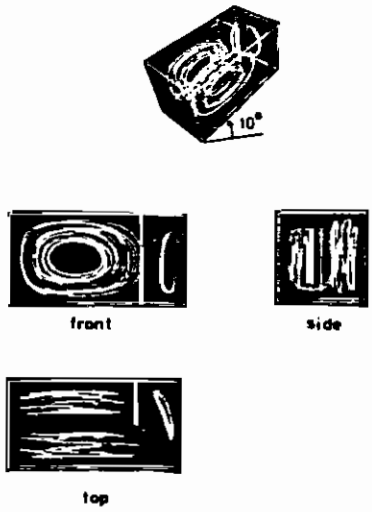

Fig. 20 Streaklines for 10π/180 rad inclinations with three-quarter location of half-extended, non-conducting baffle

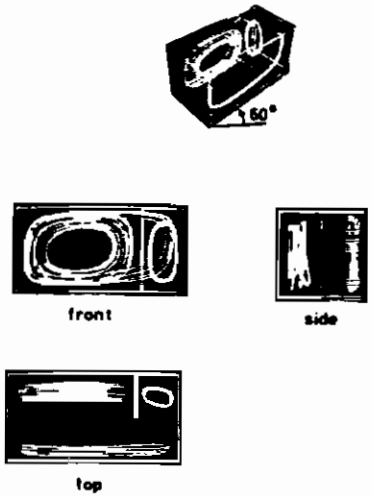

Fig. 21 Streaklines for 60π/180 rad inclination with three-quarter location of half-extended, non-conducting baffle

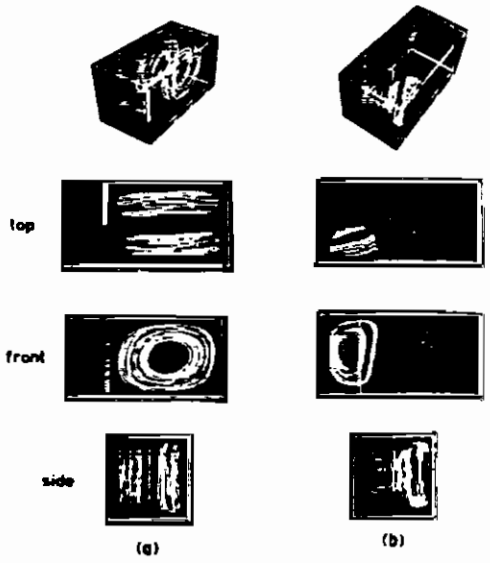

Fig. 22 Streaklines for horizontal orientation with one-quarter location of half-extended, non-conducting baffle
a) left roll-cells; b) right roll-cells

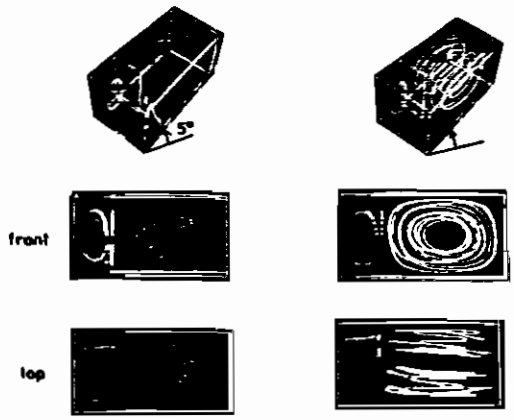

Fig. 23 Streaklines for $5\pi/180$ rad inclination with one-quarter location of half-extended, non-conducting baffle
a) left roll-cells; b) left-rear and right roll-cells

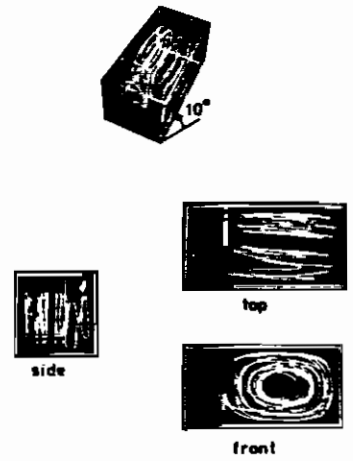

Fig. 24 Streaklines for $10\pi/180$ inclination with one-quarter location of half-extended, non-conducting baffle

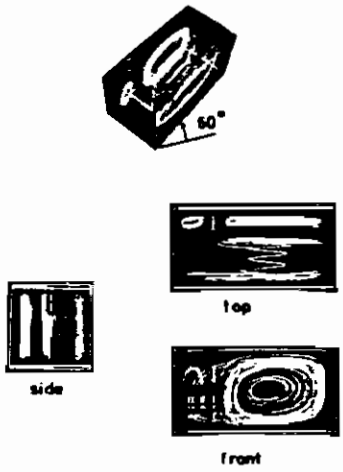

Fig. 25 Streaklines for $60\pi/180$ rad inclination with one-quarter location of half-extended, non-conducting baffle

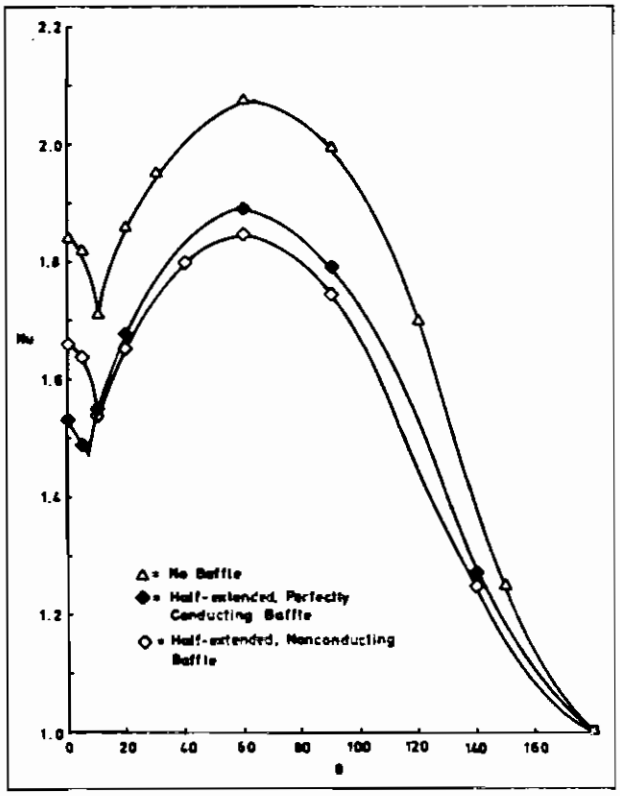

Fig. 26 Effect of perfectly-conducting and non-conducting baffles on mean Nusselt number in inclined enclosures

Nusselt numbers

The variation of the mean Nusselt number with inclination is compared in Figure 26 for no baffle, a non-conducting baffle and a perfectly conducting baffle. The Nusselt number for the case of the perfectly conducting baffle is based on the heat flux through the fluid only, since an infinite flux occurs through the baffle itself. Both the infinitely conducting and the non-conducting baffle are seen to reduce the Nusselt number significantly for all inclinations. Conduction in the baffle is seen to shift the minimum in the Nusselt number from $10\pi/180$ to $8\pi/180$ rad, to reduce the heat flux for lower inclinations and to increase it for higher ones. The reduction for lower inclinations is associated with the obliqueness of the roll-cells. The increase for higher inclinations is apparently the result of heat transfer from one roll-cell to the other by conduction normal to the thin dimension of the baffle.

The computed effect of the thermal conductivity and thickness of the baffle on the Nusselt number is shown in Figure 27 in terms of the composite variable $\lambda_r L/\lambda_f H$ indicated by eq. (2). The absence of any parametric dependence on L/H or λ_r/λ_f confirms the validity of the primary approximation leading to eq. (2), namely, a negligible temperature gradient across the baffle. This relationship also indicates that conduction across the baffle from one roll-cell to another has a greater effect on the flow pattern, and hence on the rate of heat transfer through the fluid, than conduction in the plane of the baffle.

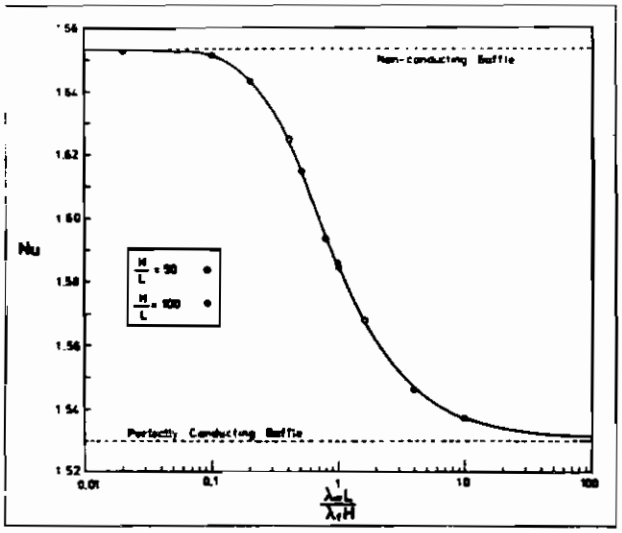

Fig. 27 Effect of finite conductivity and thickness of baffle on Nusselt number for horizontal orientation

Figure 28 shows that extension of the breadth of a nonconducting baffle has the expected effect of reducing the rate of heat transfer, but the marginal effect of the increase from a 1/2 baffle to a 7/10 baffle is small.

The effect of the location of a nonconducting baffle on the Nusselt number is illustrated in Figure 29. The two noncentral locations reduce the heat flux at small inclinations, but central location of the baffle produces the lowest flux at high inclinations, and location of the baffle in the unelevated end the greatest.

Contribution of conduction through the baffle

The results in Figures 26–28 are for heat flux through the fluid only. For baffles of finite conductivity and thickness an additional heat flux passes between the baffle and the heated and cooled surfaces. For a thickness ratio $H/L = 100$, the computed increment to the overall Nusselt number is 0.05, 0.33 and 2.5 for k_s/k_f of 10, 100 and 1000, respectively.

Conclusions

The good agreement between the computed and measured results indicates that such calculations, even with a crude grid, can be relied upon to reveal the pattern of flow.

The computed flow patterns are free from the smearing that results from diffusion and settling of the tracer particles of the experiments, and from the unavoidable anomalies in the experimental boundary conditions. The theoretical model also allowed a more systematic study of the thickness and conductivity of the baffles than was feasible experimentally.

Increasing the conductivity of the baffles radically changes the flow pattern, reduces the inclination for the minimum in the Nusselt number, reduces the heat flux through the fluid for inclinations less than the critical value and increases it for greater inclinations. The heat flux between the baffle and the heated and cooled surfaces is negligible for small conductivity ratios but becomes significant as k_s/k_f exceeds 100.

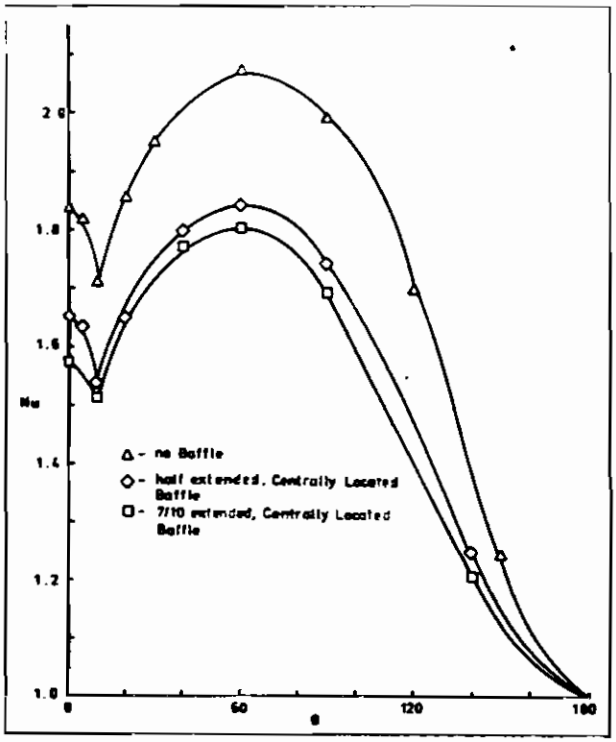

Fig. 28 Effect of extension of an non-conducting baffle on Nusselt number in inclined enclosures

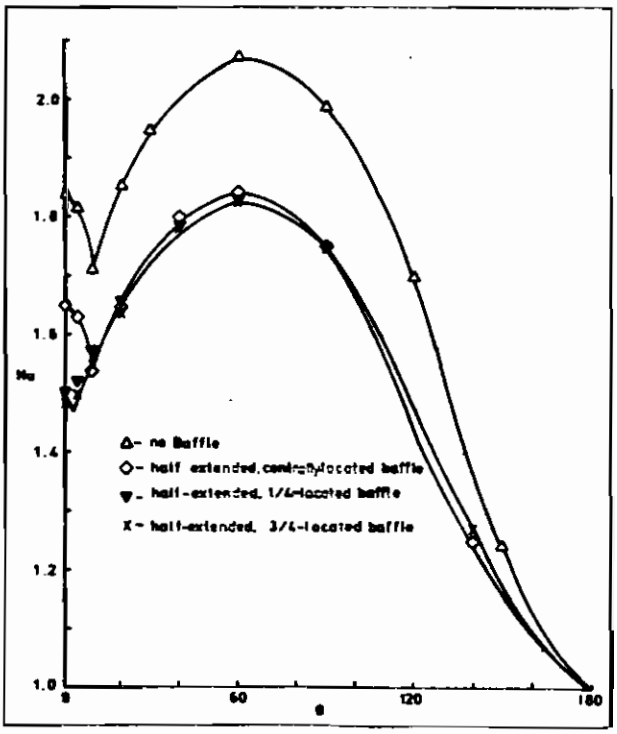

Fig. 29 Effect of location on non-conducting, half-extended baffle on Nusselt number in inclined enclosures.

The computed effects of baffle breadth and location on the pattern of circulation and the Nusselt number are similar to those described in Part I of this investigation [1], and hence need not be repeated here.

The overall conclusion of the combined experimental and theoretical investigation is that partial baffles can be used to modify the pattern of circulation and thereby reduce the heat flux due to natural convection significantly.

Acknowledgement

This work was supported in part by the U.S. Department of Energy Solar Heating and Cooling R+D Branch through Contract EM-78-04-5365, and in part by Special Research Projects on Energy Problems of Grants-in-Aid for Scientific Research, Ministry of Education, Japan. The participation of Prof. Ozoe in the work at the University of Pennsylvania was cosponsored by the Japan Society for the Promotion of Science and the U.S. National Science Foundation.

References

[1] Chao, Paul K.-B., Ozoe, H., Lior, H., and Churchill, S.W., The Effect of Partial Baffles on Natural Convection in an Inclined Rectangular Enclosure. Part I. Experimental Observations. *Chem. Eng. Fundam.* Vol. 2, 1983.

[2] Ozoe, H. Yamamoto, K., Churchill, S.W. and Sayama, H., Three-Dimensional, Numerical Analyses of Laminar Natural Convection in a Confined Fluid Heated from Below. *J. Heat Transfer*, Vol. 98C, pp. 208–207, 1976.

[3] Samuels, M.R., and Churchill, S.W., Stability of a Fluid in a Rectangular Region Heated from Below, *AIChE Jl.* Vol. 13, pp. 77–85, 1967.

[4] Yamamoto, K., Ozoe, H., Chao, P.K.-B., and Churchill, S.W., *Computers & Chem. Eng.*, Vol. 6, pp. 161–167, 1982.

Nomenclature

c	specific heat capacity of baffle, J/kg · K
g	acceleration due to gravity, m/s²
H	height of enclosure, m
L	thickness of baffle, m
Nu	$\dot{q}H/\lambda_f \Delta T$ = mean Nusselt number
Pr	$\nu/\varkappa$ = Prandtl number
$\dot{q}$	mean heat flux density through fluid, W/m²
Ra	$g\Delta\varrho H^3/\nu\varkappa\varrho$
t	time, s
T	temperature, K
x	distance in the longer horizontal dimension from the non-elevated end, m
X	x/H
y	distance in the shorter horizontal dimension from the side to which the baffle is attached, m
Y	y/H
z	distance from the cooled plate, m
Z	z/H

Greek Symbols

δ_i	finite-difference operator
θ	angle of inclination of heated surface, rad
$\varkappa$	thermal diffusivity, m²/s
λ	thermal conductivity, W/m · K
ν	kinematic viscosity, m²/s
ϱ	density, kg/m³

Supscripts

f	fluid
i,j,k	indices for baffle grid
I,J,K	indices for fluid grid
NXF	location of baffle in X-direction
NYF	location of tip of baffle in Y-direction
w	baffle